DOI: 10.13009/EUCASS2017-405

Flow Control Mechanisms of the Karman-Vortex Generator in Conical Diffuser Separation

Yang Jinwen ,Zhang Yufei* and Chen Haixin**

* *School of Aerospace Engineering, Tsinghua University*

School of Aerospace Engineering, Tsinghua University, Bejing, 100084, China

Abstract

A novel Karman-Vortex Generator (KVG) was employed to improve the pressure recovery performances in a conical diffuser with large divergence angle (29.14°). RANS/URANS/DES were used to judge and verify the effect of KVG and the Implicit Large Eddy Simulation (ILES) was set to investigate the flow control mechanisms. All the results suggested that well designed KVG could effectively promote the total pressure and static pressure recovery. The KVG could effectively suppress vortices generation near the throat, and the alternately shedding Karman-Vortexes could inject high energy fluid and enhance the fluid mixing in the separation region.

1. Introduction

As a device to convert the kinetic energy into the pressure potential, conical diffusers are widely used in the wind tunnels and turbomachinery[1]. Working in strong adeverse pressure greadient circumstances, flow seperation and total pressure distortion are common in the diffusers with great divergence angle or area ratio, which may cause energy loss and threat to flight safety. To assure the structure compact and gain better performance, modern diffuser system tend to increase the divergence angel and area ratio. Effective flow control methods were essential to assure the diffusion performance in strong adverse pressure gradient circumstances.

The flow in planar and conical diffusers have been widely researched in last decades. Patterson [2] integrated and summarized the experimental works of Gibson [3][4] and others, and suggested that the efficient diffusers should have the following total divergence angels: 6° for the square cross-section diffusers, 6~8° for the conical diffusers and 11° for a rectangular two dimensional diffuser. Azad Ram S[5] conducted a review of the experimental studies of the conical diffusers during 1966 to 1996, and elaborated their experimental research of conical diffuser with total divergence of 8°, it appeared that the flow were divided into four distinct parts: the inlet region, intermediary region I, intermediary region II and the outlet region. Mahalakshmi[6] et al. investigated the inlet flow conditions influences on the flow of two conical diffusers with half-cone angle of α=5° and α=7°. Their experiments suggested that the wake of center body has a marginal increase of the pressure recovery of the 5° diffuser. For the case of α=7°, the wake of streamline body will increase under adverse pressure gradient conditions while the wake of bluff body will have an interaction with boundary layer and the wake decay rate was arrested. Betouche[7] et al. employed the PIV measurements and Proper Orthogonal Decomposition(POD) to analysis the turbulent flow structures and energy mode in a conical diffuser with total divergence angle at 2α=16° and 2α=30°. Although their experimental Reynolds number was nearly 37000, there were obvious large scale separation in the expansion region in the case 2α=30°, and the boundary detachment enhance depends on the turbulence level with divergence angle increases.

Numerically, the conical diffuser flow was simulated with the k-ε model[1] and the algebraic Reynolds stress model (ASM)[8] in the early stage studies. These studies suggested that both the k-ε model and the ASM method could hardly simulate the complex separation flow of conical diffuser with large divergence angle. The planar diffuser with one side divergence angle of 10°[9] and 8.5°[10] was intensively studied with LES and the PIV measurements in the last 20 years, and the flow parameters of these diffusers could be standard examples to validate the numerical models and experimental devices. The researches of reference[9] and [10] suggested that the flow in the diffuser demonstrated strong separation.

Various flow control methods were conducted to reduce the total pressure losses and suppress the flow distortion in the planar and conical diffusers. The passive flow control methods were effective in diffuser separation control, and the devices were relatively simple and easy to implement. Sajeben[11] et al. used a ring shape flow control device to improve the flow separation and distortion in a conical diffuser with the total angle varied from 13° to 31°. The flow control ring of well-place and appropriate size effectively improved the total pressure recovery performances and the flow distortion in the diffusers was greatly alleviated as well. The total pressure recovery coefficient was increased about 0.03 to 0.10 and the flow distortion was decreased about 50% in the cases of the total divergence angle less than 20°. Huang Xijun[12] et al. set a circular cylinder in the upstream of a planar diffuser to suppress the flow separation, and the device effectively delayed the flow separation and diminished the separation height.

DOI: 10.13009/EUCASS2017-405

Both the ring shape flow control rail and circular cylinder will introduce unsteady span-wise Karman Vortexes before the separation region, which is different with the stream-wise vortexes generated by the traditional van type vortex generators. Chen Haixin and Zhang Yufei[13] et al. called the novel ring shape and circular cylinder shape vortex generators as a Karman Vortex Generator (KVG) and this paper follow the definition. At 2012, Chen Haixin and Zhang Yufei[13] et al. used a KVG to improve the performance of a conical diffuser with the divergence angel of 29.14°. The numerical simulation results suggested that well designed KVG improved about 1.2% of the total pressure recovery coefficient of the diffuse section. The KVG was also used to promote the performance of high lift device with large deflection angles [14]. The well designed KVG improved 18% of the maximum lift of the high lift device in the circumstances of the flection angle 55° while the van type vortex generators only gains 6% maximum lift increases.

The appropriate designed KVG shows much potential application in internal and external flow control cases, especially effective in the strong adverse pressure gradient circumstances. However, the flow control mechanisms are not clearly yet and the design principles of KVG is a key issue to be explored. In this paper, RANS (Reynolds-Averaged Navier -Stokes) / URANS (Unsteady RANS) /DES (Detached Eddy Simulation) and ILES (Implicit Large Eddy Simulation) were conducted to simulate the flow details of a baseline diffuser with the divergence angle as large as 29.14°. Effectively improved cases were also calculated as a comparison. This paper focus on the flow pattern analysis and flow field characteristics statistics to reveal the flow control mechanisms of the KVG.

2. Geometrical models and boundary conditions description

In the previous study of the research group [13], the baseline diffuser with total divergence angle of 29.14° and area ratio of 3.53 was calculated, and at least 10 KVG schemes with different size and setting places were compared. The flow control effect was directly related with the KVG settings. In this paper, the baseline diffuser and the most effective scheme in reference [13] were calculated.

The computational model of the diffuser with KVG is show in Figure 1.The baseline diffuser was the same size to the model but without the KVG. Total length of the diffuse model is 5.50m， the section before the throat is 2.05m with diameter 0.266m and the length of expansion section is 0.45m, the pipe diameter after the expansion section is 0.50m. The KVG is ring shape with its diameter of 0.02m, the detail size and location of KVG is show in Figure 2.

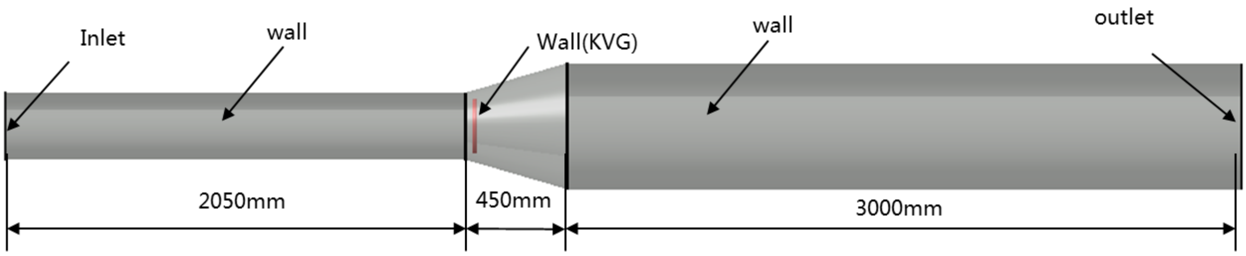

Figure 1 Calculation model of the diffuser with KVG

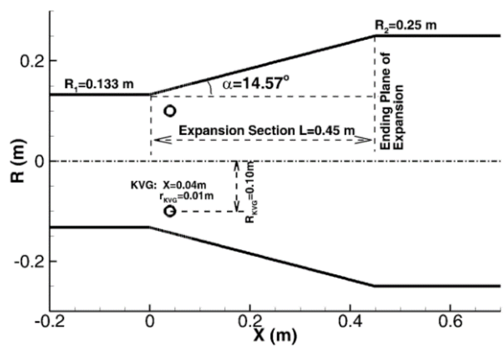

Figure 2 Detail of the diffuse section of the controlled diffuser [13]

The inlet of the diffuser was set total pressure (118600Pa) and total temperature (930K) boundary condition， the outlet section was set the static pressure (111482Pa) boundary condition, and the other walls of the diffuser and the KVG was set no slip wall. The Reynolds number of the diffuser throat was 9.31×10^5, and the Mach number was about 0.45 in the expansion section, and the flow in the whole diffuser was subsonic. Total pressure recovery coefficient and static recovery coefficient were key parameters to evaluate the diffuse performance of the diffuser. Total pressure recovery coefficient C_{TR} and static pressure coefficient C_{PR} was calculated by the formula (1) and (2).

DOI: 10.13009/EUCASS2017-405

The C_{TR} characterized the energy loss of the expansion process and C_{SR} represents the performance of diffuser convert kinetic energy to pressure potential. $\overline{P_{t1}}$, $\overline{P_1}$ and $\overline{P_{t2}}$, $\overline{P_2}$ respectively represented the averaged total pressure and averaged static pressure of the throat profile and the end profile of the expansion section.

$$C_{TR} = (\overline{P}_{t1} - \overline{P}_{t2}) / \overline{P}_{t1} \quad \textbf{(1)}$$

$$C_{SR} = (\overline{p}_2 - \overline{p}_1) / \tfrac{1}{2}\rho_\infty v_\infty{}^2 \quad \textbf{(2)}$$

3. Grid settings and numerical methods

The study conducted RANS/URANS/DES and ILES to simulate the flow in the diffuser, and different simulation methods required different grid and adequate numerical schemes. Six sets of structural grids were conducted for combinations of different simulation methods and diffuser models. All the grids were structural grids and the maximum Y-plus of the first layer near the wall were less than 1.0. The detail of grid number and distributions of different cases are shown in Table 1. The detail of the grid distribution of ILES case is show in Figure 3.

Table 1 Grid parameters of the calculation

CASE	Simulation Method	Numerical Schemes	Grid Around KVG(nx,nR,nθ)	Grid Distribution (nx,nR,nθ)	Total Grid	Maximum Y-plus
Baseline	ILES	SLAU+MDCD	-	390×176×240	20,296,000	0.85
KVG	ILES	SLAU+MDCD	68×208×240	390×176×240	24,284,000	0.95
Baseline	DES	SLAU+MDCD	-	328×146×200	11,851,000	0.6
KVG	DES	SLAU+MDCD	56×192×200	328×146×200	13,800,000	0.8
Baseline	URANS	SLAU+WENO		280×120×160	6,783,000	0.6
KVG	URANS	SLAU+WENO	48×144×160	280×120×160	7,603,000	0.9

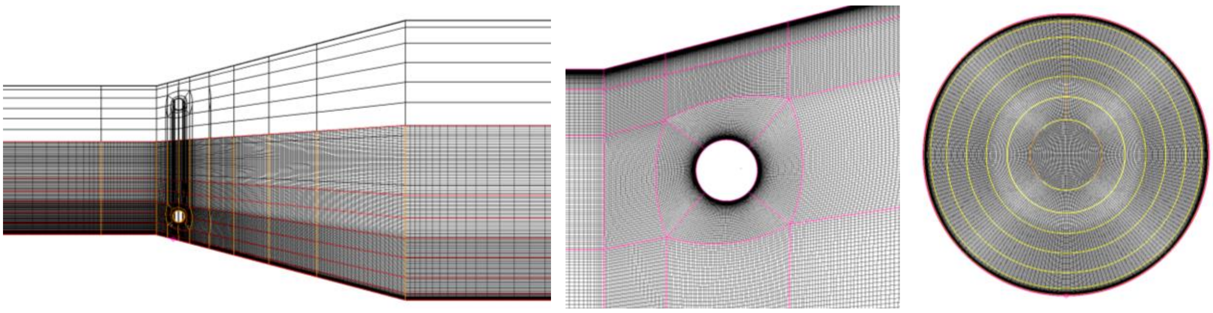

Figure 3 Grid details of the ILES of Controlled case

An in house general-purpose Navier-Stokes equation solver NSAWET (Navier-Stokes Analysis based on Window-Embedment Technology) was employed in this study, and the solver possesses reliable and stable accuracy in solving relevant problems[13][15][16][17]. It is based on finite volume method with multi-block structured grid and is fully parallelized using the Message Passing Interface (MPI) library. The RANS/URANS simulation could be used to estimate the averaged flow field and verify the performance of the flow control combinations at a low cost, while it's hard to describe the complex flow details of the diffuser[1][9]. DES and ILES was employed to gain the flow details in case of investigating the flow control mechanisms of the diffuser with KVG.The RANS/URANS and DES calculations in this paper are based on the famous SST *k-ω* model [18], and the model gained very wide applications in solving engineering problems and doing researches. The ILES method employed in the paper was combined with SLAU scheme for Riemann Solver and the MDCD scheme for reconstruction, and it possesses good performances in the unsteady simulations [17] [19].

The inviscid numerical flux is calculated by the Simple Low-dissipation AUSM (SLAU) scheme [20]. The scheme is featured with needn't tunable parameters in low Mach number cases compared with other all-speed schemes. At the same time, SLAU scheme possesses a robustness performance of AUSM family at high Mach number condition. The scheme could effective against shock-induced anomalies and odd–even decoupling problems at high Mach number cases. The numerical flux of SLAU scheme is written in the following formulas (3) ~ (7). The detail features and the formulas was elaborated in the reference [20].

DOI: 10.13009/EUCASS2017-405

$$\tilde{F} = \frac{\dot{m} + |\dot{m}|}{2}\Phi^{+} + \frac{\dot{m} - |\dot{m}|}{2}\Phi^{-} + \tilde{p}\vec{n} \tag{3}$$

$$\Phi = \left(1, u, v, w, h\right)^{T} \tag{4}$$

$$h = \left(e + p\right) / \rho \tag{5}$$

$$\vec{n} = \left(0, n_x, n_y, n_z, 0\right)^{T} \tag{6}$$

$$\tilde{p} = \frac{p^{+} + p^{-}}{2} + \frac{\beta^{+} - \beta^{-}}{2}\left(p^{+} - p^{-}\right) + f_p \cdot \left(\beta^{+} + \beta^{-} - 1\right)\frac{p^{+} + p^{-}}{2} \tag{7}$$

For the reconstruction processes, the RANS/URANS used WENO scheme while the DES and ILES were based the fourth-order Minimum Dispersion and Controllable Dissipation (MDCD) scheme [21], and the differences was mainly to assure the calculation stability. MDCD scheme employed weight factor to combine the fourth-order linear and nonlinear schemes, the complete expression is in the following formula (8) ~ (11). The variable ϕ in the formula represents the conservative variable and σ refers to the weight factor of the liner or nonlinear parts.

$$\phi_{j+1/2}^{MDCD} = \sigma_{j+1/2}\phi_{j+1/2}^{linear} + \left(1 - \sigma_{j+1/2}\right)\phi_{j+1/2}^{non-linear} \tag{8}$$

$$\sigma_{j+1/2} = \min\left(1, r_{j+1/2}/r_c\right), r_{j+1/2} = \min\left(r_j, r_{j+1}\right),\ r_c = 0.4 \tag{9}$$

$$r_j = \frac{\left|2\Delta\phi_{j+1/2}\Delta\phi_{j-1/2}\right| + \varepsilon}{\left(\Delta\phi_{j+1/2}\right)^2 + \left(\Delta\phi_{j-1/2}\right)^2 + \varepsilon},\ \varepsilon = 5.6\times10^{-4} \tag{10}$$

$$\Delta\phi_{j+1/2} = \phi_{j+1} - \phi_j \tag{11}$$

The WENO scheme based on three-cell candidate stencils could be described as the formula (12) .The variable c_k and w_k represents the liner weight and the non-liner weight factor. In the present research, the liner weight factor c_k is determined by two free parameters γ_{disp} and γ_{diss}, these variables could adjust the dispersion and dissipation respectively, the expression of c_k is shown in the formula (13). The recommended values γ_{disp}=0.046 andγ_{diss}=0.01 are used in the present research. The non-liner weight factor w_k could be acquired by the formula (14), and the calculation expression is similar to the WENO scheme in case of p_0=1. The details of the expression and the variables meaning could be found in reference [21].

$$\phi_{j+1/2}^{linear} = \sum_{k=0}^{3} c_k\phi_{j+1/2}^{k},\ \phi_{j+1/2}^{non-linear} = \sum_{k=0}^{3} w_k\phi_{j+1/2}^{k},\ k = 0,1,2,3. \tag{12}$$

$$\begin{aligned} c_0 &= \frac{3}{2}\gamma_{disp} + \frac{3}{2}\gamma_{diss}, \\ c_1 &= \frac{1}{2} - \frac{3}{2}\gamma_{disp} + \frac{9}{2}\gamma_{diss}, \\ c_2 &= \frac{1}{2} - \frac{3}{2}\gamma_{disp} - \frac{9}{2}\gamma_{diss}, \\ c_3 &= \frac{3}{2}\gamma_{disp} - \frac{3}{2}\gamma_{diss}. \end{aligned} \tag{13}$$

$$w_k = \left[\frac{c_k}{\varepsilon + IS_k}\right] \Bigg/ \sum_{k=0}^{3}\left[\frac{c_k}{\varepsilon + IS_k}\right],\ \varepsilon = 10^{-6} \tag{14}$$

The detailed schemes and the unsteady simulation performances of the ILES method was elaborated in reference [19]. The ILES combined with the SLAU and MDCD schemes possesses robustness and good resolution in multi-scale flow simulations. All the calculations applied the fully implicit Lower-Upper Symmetric-Gauss-Seidel (LU-SGS) scheme for time march, and the dual-time stepping method was adopted to obtain second order accuracy.

4. Results and discussion

4.1 Transient flow field analysis

The flow in present diffuser is characterized by strong separation and multiscale vortexes. Figure 4 presents the instantaneous total pressure distribution of the diffuser with and without KVG of the symmetry profile z=0.

DOI: 10.13009/EUCASS2017-405

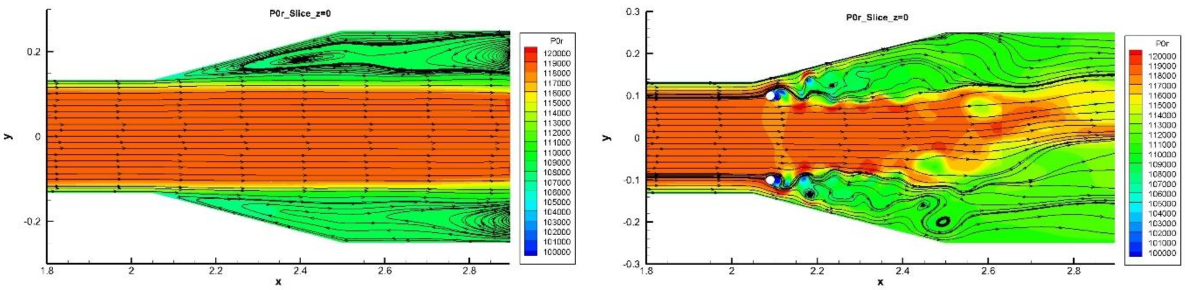

(a) URANS result of the instantaneous total pressure distribution (Left :Baseline Right :Controlled)

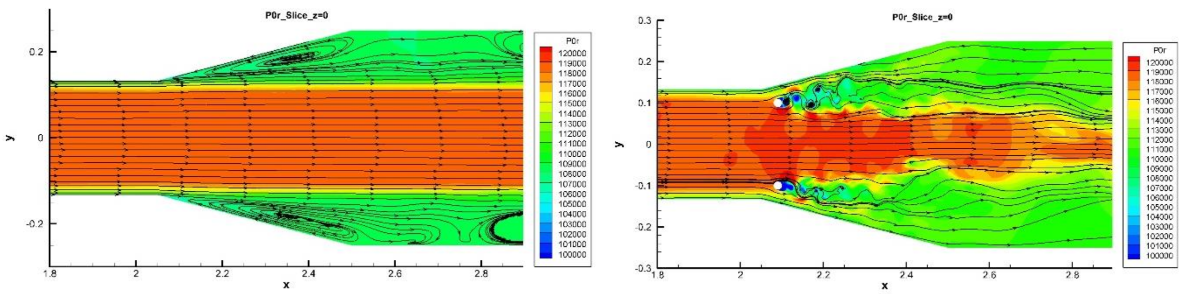

(b) DES result of the instantaneous total pressure distribution (Left :Baseline Right :Controlled)

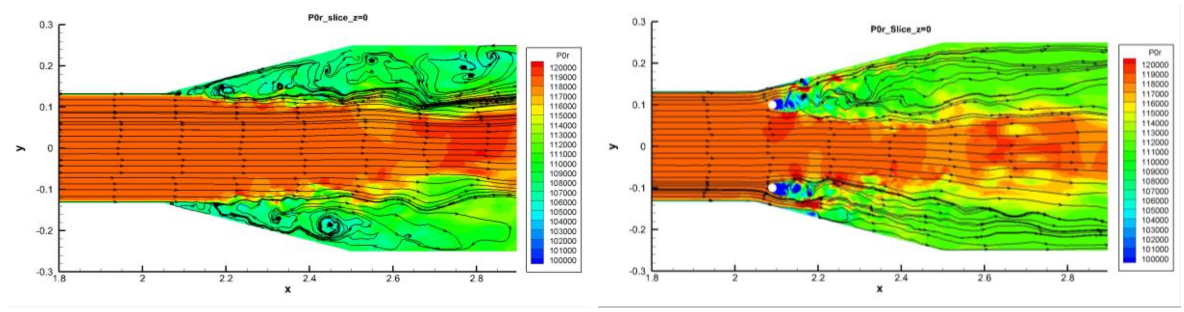

(c) ILES result of the instantaneous total pressure distribution (Left :Baseline Right :Controlled)

Figure 4 Instantaneous total pressure distribution results of slice z=0

For the cases of baseline diffuser, the total pressure distribution and flow pattern of DES was similar to URANS, there were only large scale separation in expansion section near the wall, while the result of ILES resolve the multi-scale eddies. The flow in the diffuser is physically unsteady and multi-scale, therefore the flow details of ILES was physical reliable and could capture more flow details. All the simulation results indicate that the total pressure near the expansion boundary was obviously lower than the core region, and velocity distributed irregularly in the expansion region. Energy loss and total pressure distortion was obvious in the baseline diffuser.

When comes to the diffuser equipped well designed KVG, all the simulation results indicated that Karman vortexes generated and shedding alternately after the ring shape KVG. The wake of the KVG directly interacted with the near wall separation region and the flow was much smoother than the uncontrolled cases. In case of the total pressure differences between the near wall and core region decrease and the flow was smoother, the total pressure recovery performance and distortion performance was tend to be improved.

The Figure 5 illustrates ILES results of the streamwise velocity contours of the baseline diffuser and the controlled case at profile z=0. The streamwise velocity U_n was non-dimensionalized by the inlet streamwise velocity U_0. The U_n of the deep blue zone is negative and it refers the back flow. There were large scale back flow in the near wall region of the baseline diffuser, while the near wall velocity of the controlled diffuser was positive and the flow was smooth. Comparing the velocity of the baseline diffuser and the controlled cases, the flow near the throat section was greatly changed with the effect of KVG. The flow near the throat retarded and became instability with the effect of geometry change in the near wall region and generate small eddies. Due to the adverse pressure gradient increases in the expansion process, and the small eddies gradually developed to large scale vortexes and present obvious separation. For the controlled diffuser, the ring shape KVG accelerate the flow near the throat, and the fluid with great momentum suppressed the small eddies generation near the wall region and inject energy to the expansion region. When the fluid flow around the ring shape KVG, there will be alternatively shedding Karman-Vortexes. The

DOI: 10.13009/EUCASS2017-405

Karman-Vortexes would inject some high energy fluid to the expansion region as well, and the wake of KVG could effectively mix the high energy flow in the core region and the low energy flow near the expansion wall region. The comprehensive effects of the KVG effectively alleviated the large scale separation in the expansion section and make flow more evenly.

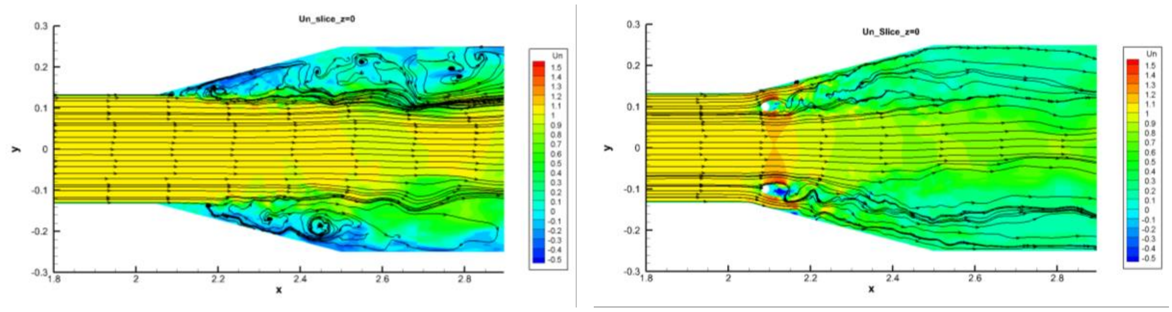

Figure 5 ILES results of instantaneous streamwise velocity distribution of slice z=0 (Left: Baseline Right: controlled)

Contours of Q criterion of the symmetry plane z=0 was presented in following Figure 6. The DES results was quite similar to the URANS results. Both of the URANS and DES method could hardly resolve the small scale vortices in the baseline diffuser, while the ILES results could depict the flow detail of baseline diffuser. The contours of the Q criterion visually described the vortices generation and evolution processes of the baseline diffuser, and vividly depict the Karman-Vortexes generated by the KVG interacted with large scale separations.

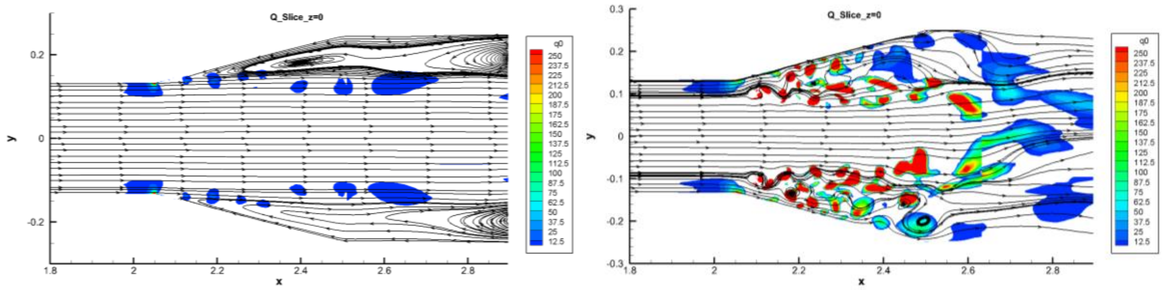

(a) URANS results of instantaneous Q criterion distribution of slice z=0

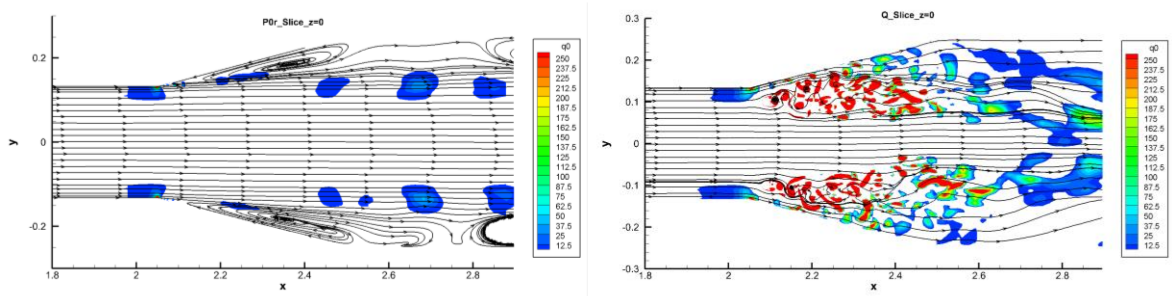

(b) DES results of instantaneous Q criterion distribution of slice z=0

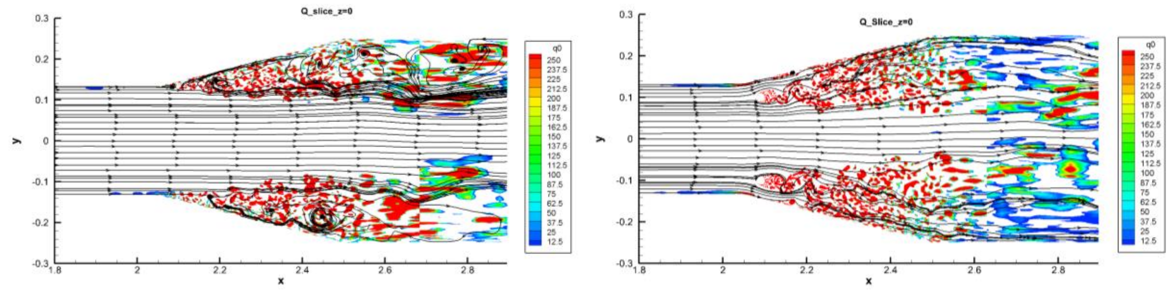

(c) ILES results of instantaneous Q criterion distribution of slice z=0

Figure 6 ILES results of instantaneous Q criterion distribution of slice z=0

DOI: 10.13009/EUCASS2017-405

4.2 Time averaged flow field analysis

Time averaged analysis was conducted to confirm and measure the effect of KVG. The Figure 7 illustrated the averaged total pressure distribution of different simulation methods of the symmetry profile z=0. The time averaged total pressure distribution of the ILES results of the profile x=2.50 was presented as well.

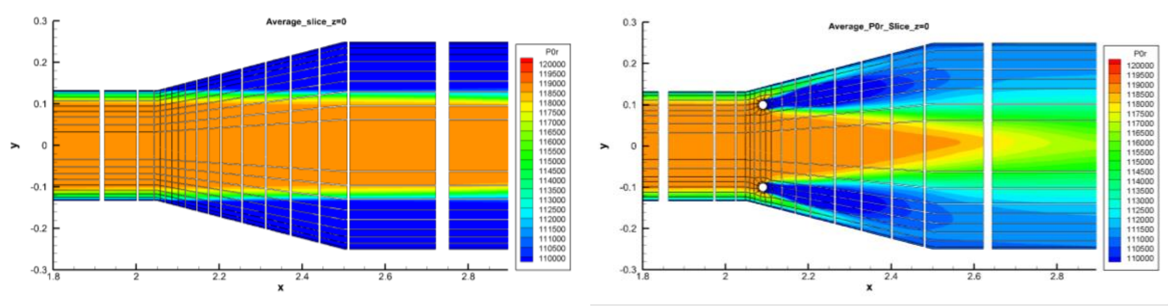

（a）URANS result of the time averaged total pressure distribution of profile z=0(Left: Baseline Right: Controlled)

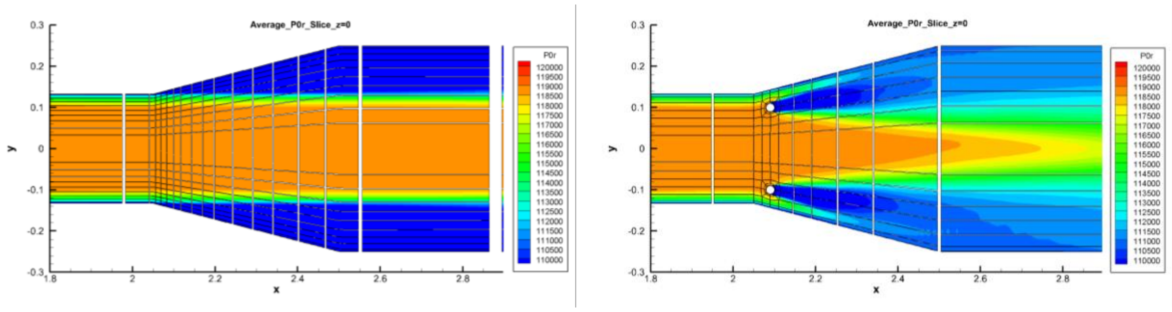

（b）DES result of the time averaged total pressure distribution of profile z=0 (Left: Baseline Right: Controlled)

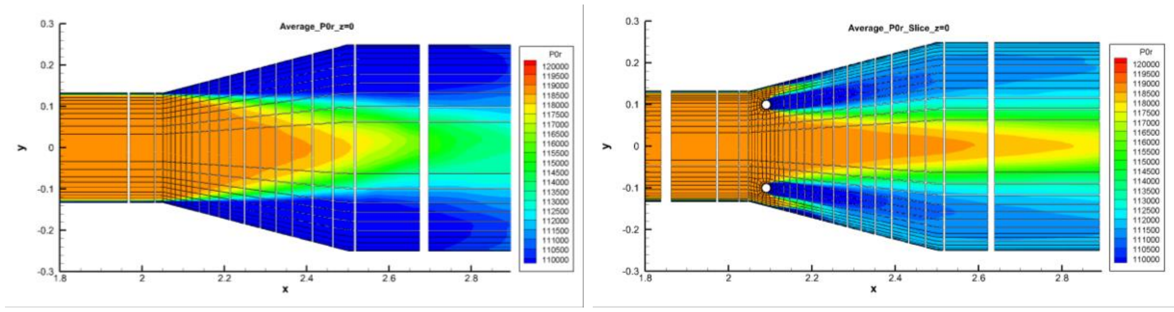

（c）ILES result of the time averaged total pressure distribution profile of z=0 (Left: Baseline Right: Controlled)

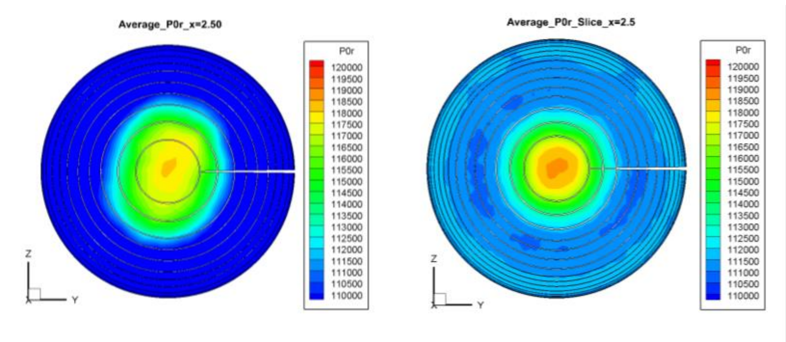

（d）ILES result of the time averaged total pressure distribution at the end of the expansion section (Left: Baseline Right: Controlled)

Figure 7 Time averaged total pressure distribution results of different simulation methods

DOI: 10.13009/EUCASS2017-405

For the baseline diffuser cases, the time averaged total pressure of the expansion section end were close to annual distribution, and the total pressure in the core area was obviously greater than the near wall regions. The total pressure distribution of the simulations comply with the basic physicals of the conical diffuse flow. The results of the URANS and DES were quite similar, but they underestimate the total pressure loss compared with the ILES results, the main reasons may be the grid resolution and simulation method limit.

For the controlled cases, the total pressure distribution of the expansion section end were annual distribution as well. The total pressure differences between the near wall zones and the core was greatly diminished with the effect of KVG. The total pressure of near wall region close to the throat section was greater than the baseline diffuser, indicating that the KVG had consistently suppress the shear instability dominated vortices generation. The alternately shedding Karman vortexes injected kinetic and might comprehensive reacted to the separation eddies to promote the total pressure of the near wall region. There were obviously low energy region in the wake of the KVG, it indicates that the KVG would generate Karman-Vortexes and enhanced energy exchange. The total pressure of the expansion section was obvious greater than the baseline diffuser, indicating that the KVG was effective in improving the total recovery performance and alleviate distortion. The calculation discrepancies between different simulation methods was relative less compared with the baseline simulations.

Total pressure recovery coefficient and static pressure recovery coefficient was calculated in the basis of the time averaged results, and the consequences was shown in Table 2. The present calculations had the same calculation model to reference [13], and Table 2 compared the present results with the reference. The static pressure recovery coefficient and the total recovery coefficient agreed well with the reference except the ILES result of the baseline diffuser. All the results indicate that the KVG was effective to improve both the total and static pressure recovery performance. The pressure recovery performances result of ILES was less than the URANS and DES, the statistic results indicate that the URANS and DES may underestimate the pressure loss, while the improvement of the total pressure was quite close in different cases. The total pressure recovery coefficient was improved 0.81% for the URANS and about 1.00% for the DES and ILES, and the improvement was a little less than the reference [13]. Although the URANS and DES method could hardly depict the flow detail of the flow field, while they can be used to verify the flow control effect at a low cost.

Table 2 Pressure recovery performances statistics

Data Source	Configurations	Computational Method	Static Pressure Recovery coefficient C_{SR}	Total Pressure Recovery coefficient C_{TR}
Reference[13]	Baseline diffuser	URANS	0.2465	93.99%
Present	Baseline diffuser	URANS	0.23023	94.73%
Reference[13]	Baseline diffuser	DES	0.2394	93.85%
Present	Baseline diffuser	DES	0.2190	94.67%
Present	Baseline diffuser	ILES	0.0840	93.52%
Reference[13]	Controlled	URANS	0.4937	95.23%
Present	Controlled	URANS	0.4493	95.54%
Reference[13]	Controlled	DES	0.4732	94.88%
Present	Controlled	DES	0.4601	95.67%
Reference[13]	Controlled	DDES	0.5028	95.09%
Present	Controlled	ILES	0.4645	94.54%

5. Conclusions

The novel Karman Vortex Generator shows much potential in both internal and external flow control. This paper employed RANS/URANS/DES and ILES methods to investigate the flow control mechanisms in a conical diffuser. From the calculation and analysis, we can draw the following conclusions.

(1) Well designed KVG showed positive effect in improving both the total pressure recovery and static pressure recovery performances of a conical diffuser with large divergence angle. The total pressure recovery coefficient was improved nearly 1% in the calculation cases and the result agreed well with the previous research.

(2) The flow in the diffuser demonstrated complex three dimensional character. There were large scale separations and multi-scale vortices in the expansion section near wall region. The ring shape KVG could accelerated the flow

DOI: 10.13009/EUCASS2017-405

near the expansion start point and the high energy flow constantly suppress the vortices generation near the throat. The alternatively shedding Karman vortexes could inject high energy fluid to the expansion region, and the wake could effectively mix the high speed flow in the core region and the separation flow near the expansion wall region.

(3) The URANS and DES method could hardly depict the complex unsteady flow of the baseline diffuser, while they can be used to verify the flow control effect at a low cost.

References

[1] Lai, Y. G., So, R. M. C., & Hwang, B. C. 1989. Calculation of planar and conical diffuser flows. *AIAA journal*, 27(5), 542-548.

[2] Patterson, G. N. 1938. Modern diffuser design: The efficient transformation of kinetic energy to pressure. *Aircraft Engineering and Aerospace Technology*, 10(9), 267-273.

[3] Gibson, A. H. 1910. On the flow of water through pipes and passages having converging or diverging boundaries. Proceedings of the Royal Society of London. Series A, Containing Papers of a Mathematical and Physical Character, 83(563), 366-378.

[4] Gibson, A. H. 1912. V.—On the Resistance to Flow of Water through Pipes or Passages having Divergent Boundaries. Transactions of the Royal Society of Edinburgh, 48(01), 97-116.

[5] Azad, R. S. 1996. Turbulent flow in a conical diffuser: A review. Experimental Thermal and Fluid Science, 13(4), 318-337.

[6] Mahalakshmi, N. V., Krithiga, G., Sandhya, S., Vikraman, J., & Ganesan, V. 2007. Experimental investigations of flow through conical diffusers with and without wake type velocity distortions at inlet. *Experimental Thermal and Fluid Science*, 32(1), 133-157.

[7] Betouche, E. B., Aloui, F., & Legrand, J. 2016. Turbulent Flows Structures Crossing Conical Diffusers: Angle Effect Analysis using PIV Technique and POD for Post-Processing. *Journal of Applied Fluid Mechanics*, Vol. 9, Special Issue 1, pp. 19-29.

[8] Cho, N. H., & Fletcher, C. A. J. 1991. Computation of turbulent conical diffuser flows using a non-orthogonal grid system. *Computers & Fluids*, *19*(3-4), 347-361.

[9] Kaltenbach, H. J., Fatica, M., Mittal, R., Lund, T. S., & Moin, P. 1999. Study of flow in a planar asymmetric diffuser using large-eddy simulation. *Journal of Fluid Mechanics*, *390*, 151-185.

[10] Törnblom, O., Lindgren, B., & Johansson, A. V. 2009. The separating flow in a plane asymmetric diffuser with 8.5 degree opening angle: mean flow and turbulence statistics, temporal behaviour and flow structures. *Journal of Fluid Mechanics*, *636*, pp:337-370.

[11] Sajben, M., Chen, C. P., & Kroutil, J. C. 1977. A new passive boundary-layer control device. *Journal of Aircraft*, *14*(7), 654-660.

[12] Huang X J, Bao F, D J Z and Xiao C S. 1988. A Study on Separation Flow Control of Diffuser. *Acta Aeronautics et Astronautic Sinica*, *9(2)*, 35-40.

[13] Zhang, Y., Chen, H., & Fu, S. 2012. A Karman-Vortex Generator for passive separation control in a conical diffuser. *SCIENCE CHINA Physics, Mechanics & Astronomy*, *55*(5), 828-836.

[14] Veldhuis, L. L. M., et al. 2012. Novel passive and active flow control for high lift. 28th ICAS Proceedings, 1-17.

[15] Zhang, Y., Chen, H., Zhang, M., Zhang, M., Li, Z., & Fu, S. (2014). Performance prediction of conical nozzle using Navier–Stokes computation. *Journal of Propulsion and Power*, *31*(1), 192-203.

[16] Zhang, Y., Chen, H., Fu, S., Zhang, M., & Zhang, M. 2015. Drag prediction method of powered-on civil aircraft based on thrust drag bookkeeping. *Chinese Journal of Aeronautics*, *28*(4), 1023-1033.

[17] Chen, H., Li, Z., & Zhang, Y. 2016. U or V Shape: Dissipation Effects on Cylinder Flow Implicit Large-Eddy Simulation. *AIAA Journal.55(2)*, 459-473

[18] Menter, F. R., Kuntz, M., & Langtry, R. 2003. Ten years of industrial experience with the SST turbulence model. *Turbulence, Heat and Mass Transfer*, *4*(1), 625-632.

[19] Li, Z., Zhang, Y., & Chen, H. 2015. A low dissipation numerical scheme for implicit large eddy simulation. *Computers & Fluids*, *117*, 233-246.

[20] Shima, E., & Kitamura, K. 2011. Parameter-free simple low-dissipation ausm-family scheme for all speeds. *AIAA Journal*, *49*(8), 1693-1709.

[21] Wang, Q. J., Ren, Y. X., Sun, Z. S., & Sun, Y. T. 2013. Low dispersion finite volume scheme based on reconstruction with minimized dispersion and controllable dissipation. *Science China Physics, Mechanics & Astronomy*, *56*(2), 423-431.